Supplemental Table 1

Group similarity comparisons	miRNA list
Eutopic > Ectopic Ectopic > Normal	has-miR-206 hsa-miR-29c-3p hsa-miR-139-3p hsa-let-7a-3p hsa-miR-95-3p hsa-miR-29b-3p hsa-miR-495-3p hsa-miR-136-3p hsa-miR-887-3p hsa-miR-381-3p hsa-miR-100-5p hsa-miR-193b-3p hsa-miR-335-5p hsa-miR-411-5p
Normal > Ectopic Ectopic > Eutopic	hsa-miR-1266-5p hsa-miR-200c-3p hsa-miR-200a-3p hsa-miR-20b-5p hsa-miR-200a-5p hsa-miR-96-5p
Ectopic > Normal Eutopic > Normal	hsa-miR-451a hsa-miR-144-5p
Ectopic > Eutopic Eutopic > Normal	hsa-miR-486-5p
Control > Patient plasma & Normal > Ectopic & Ectopic > Eutopic	hsa-miR-375 hsa-miR-30d-5p
Control > Patient plasma & Eutopic > Ectopic & Ectopic > Normal	hsa-miR-27a-3p

List of all miRNAs differentially expressed in multiple sample and comparison groups.

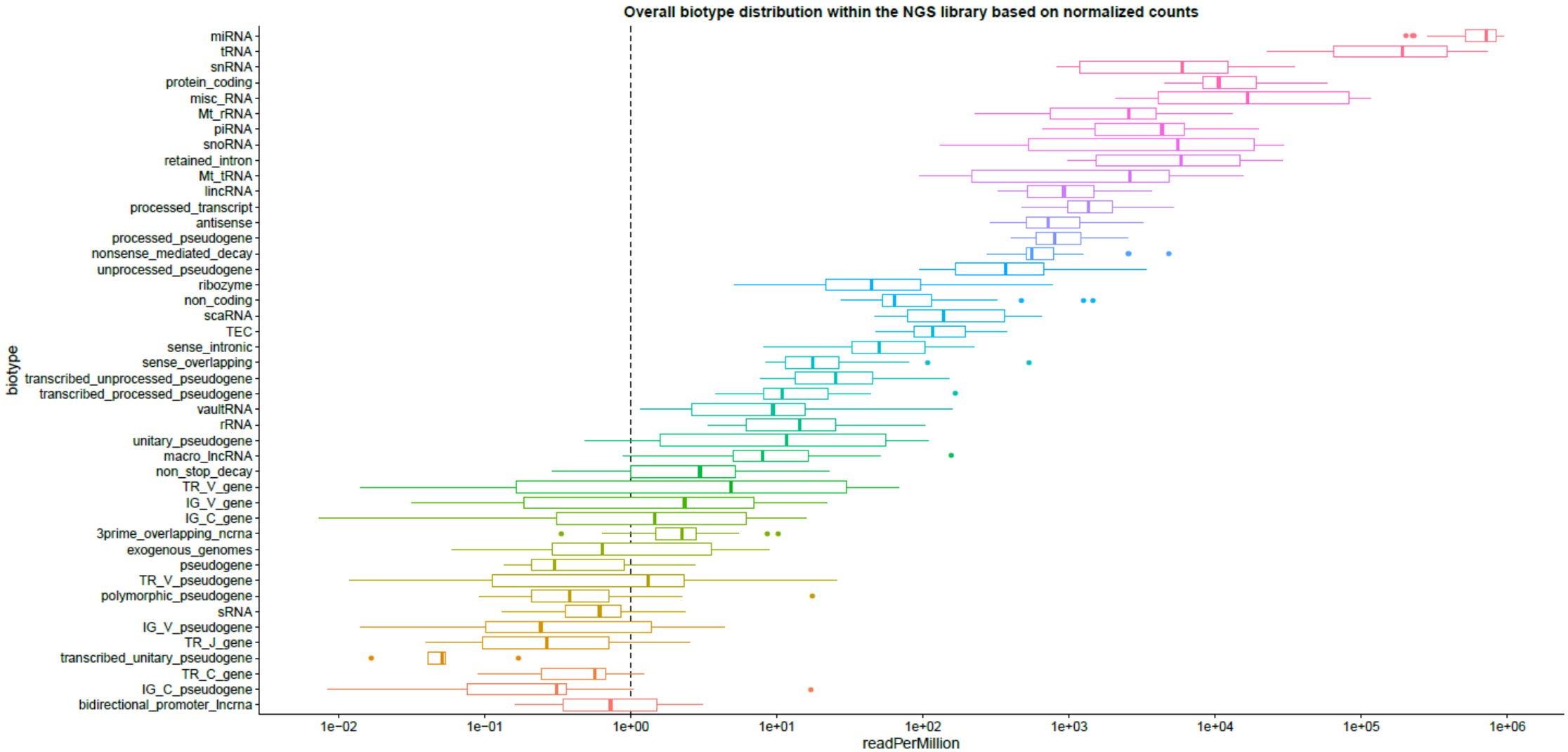

Supplemental Figure 1: SmallRNAseq overall biotype distribution within the NGS library based on raw read counts. Biotype distribution analysis reveals highest counts as miRNAs (top pink line), followed by tRNA, snRNA and protein-coding. pi-, sno, and linc-RNAs were the seventh, eighth and eleventh most abundant small RNA species in the distribution map, respectively. Pseudogenes ranging from TR_V to IG_C type were the least abundantly distributed (olive colour to orange-red near bottom of the map) and bidirectional promoter lncRNAs were the least abundantly distributed in the NGS library. Analysis provides biotype fractions and their proportions across all samples in the NGS library. Data presented as mean +/- SEM.

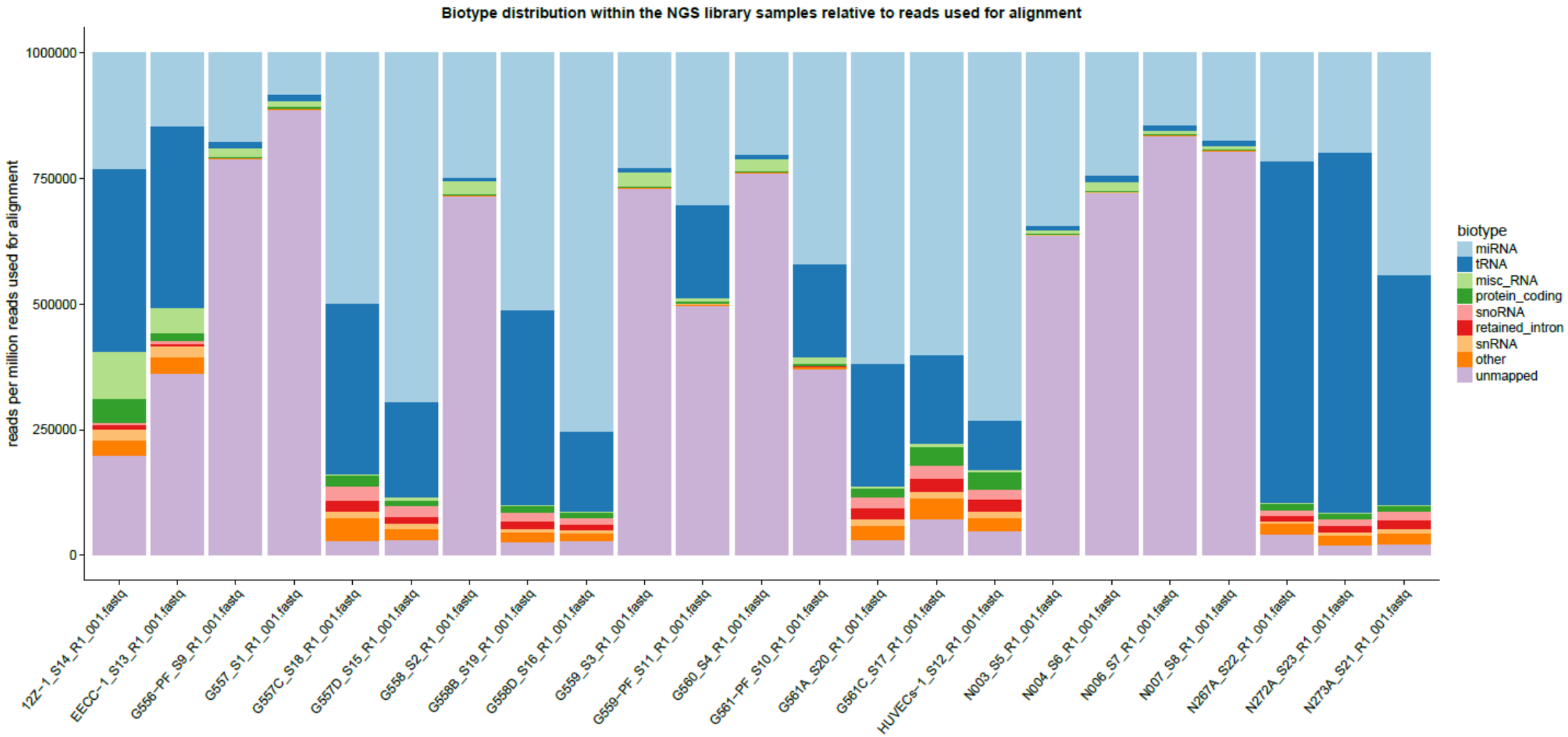

Supplemental Figure 2: SmallRNAseq overall biotype distribution within the NGS library relative to mapped reads. Biotype distribution analysis reveals highest miRNA as the highest biotype among all endometriosis lesion and eutopic endometrium from endometriosis patients as well as normal endometrium from fertile healthy controls (light blue). Plasma from endometriosis patients has higher tRNA distribution (dark blue bar) than plasma from control patients. The endometriotic epithelial and endometrial epithelial carcinoma cell lines (12Z and EECC) had higher overall tRNA biotype distribution than miRNA, while the HUVECs had lower tRNA and higher miRNA distribution. Analysis provides biotype fractions within each sample as well as between samples. n = 3 independently derived samples (pooled; cell culture derived samples), n = 4 biological samples/group (patient specimens)

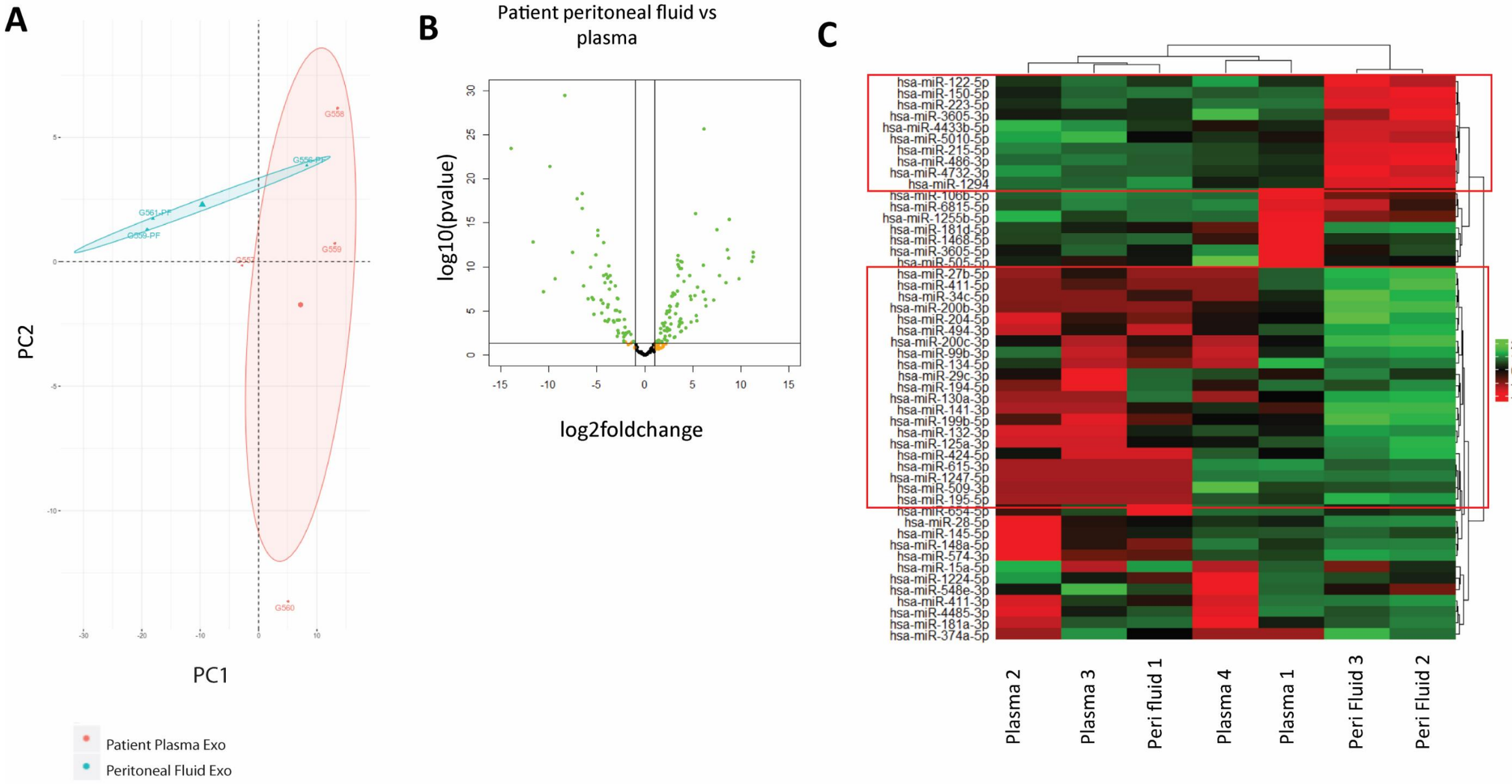

Supplemental Figure 3. Small-RNA species analysis using next-generation sequencing platform revealed unique miRNA signatures implicated in endometriosis pathogenesis & unique miRNA expression across patient peritoneal fluid and plasma extracellular vesicle (EV) sample types. Principle component analysis (PCA) of Patient plasma vs peritoneal fluid derived EVs (PC1 = 65.3%, PC2 = 13.9%) reveal demarcations between each group (A). Differentially expressed miRs between patient peritoneal fluid and plasma (A-C). With the exception of one peritoneal fluid sample (#1; C), the groupings were profound, and two clusters of DE miRs were identified (C; red boxes). The top and bottom clusters included 10 and 21 DE miRs, respectively. n = 4 biological samples/group for plasma EV samples and n = 3 biological samples/group for peritoneal fluid EV samples.

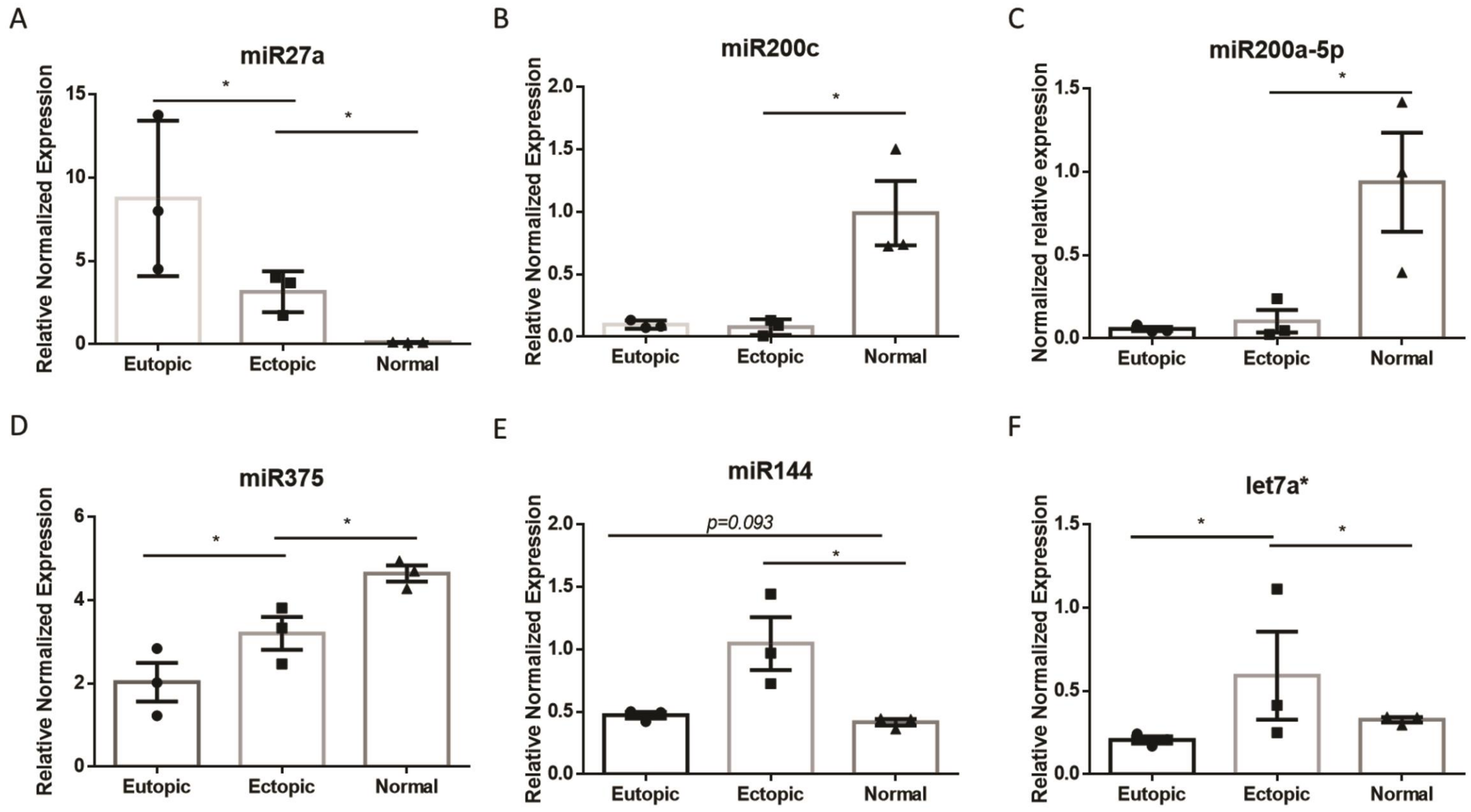

Supplemental Figure 4. Validation of differentially expressed miRNAs in multiple sample and comparison groups using quantitative PCR. miR27a is upregulated in EVs from eutopic endometrium, and ectopic endometriosis compared to normal endometrium (A), and miR200c, -200a-5p, -375 are upregulated in EVs from normal endometrium compared to ectopic endometriosis (B-D). miR-375 is also upregulated in EVs from ectopic endometriosis compared to eutopic endometrium (D). miR144 and let7a are upregulated in ectopic endometriosis EVs compared to normal endometrium (E-F), and let7a is also downregulated in eutopic endometrium compared to ectopic endometriosis EVs (F). Comparisons made using one-way ANOVA. n = 3 biological replicates/group.

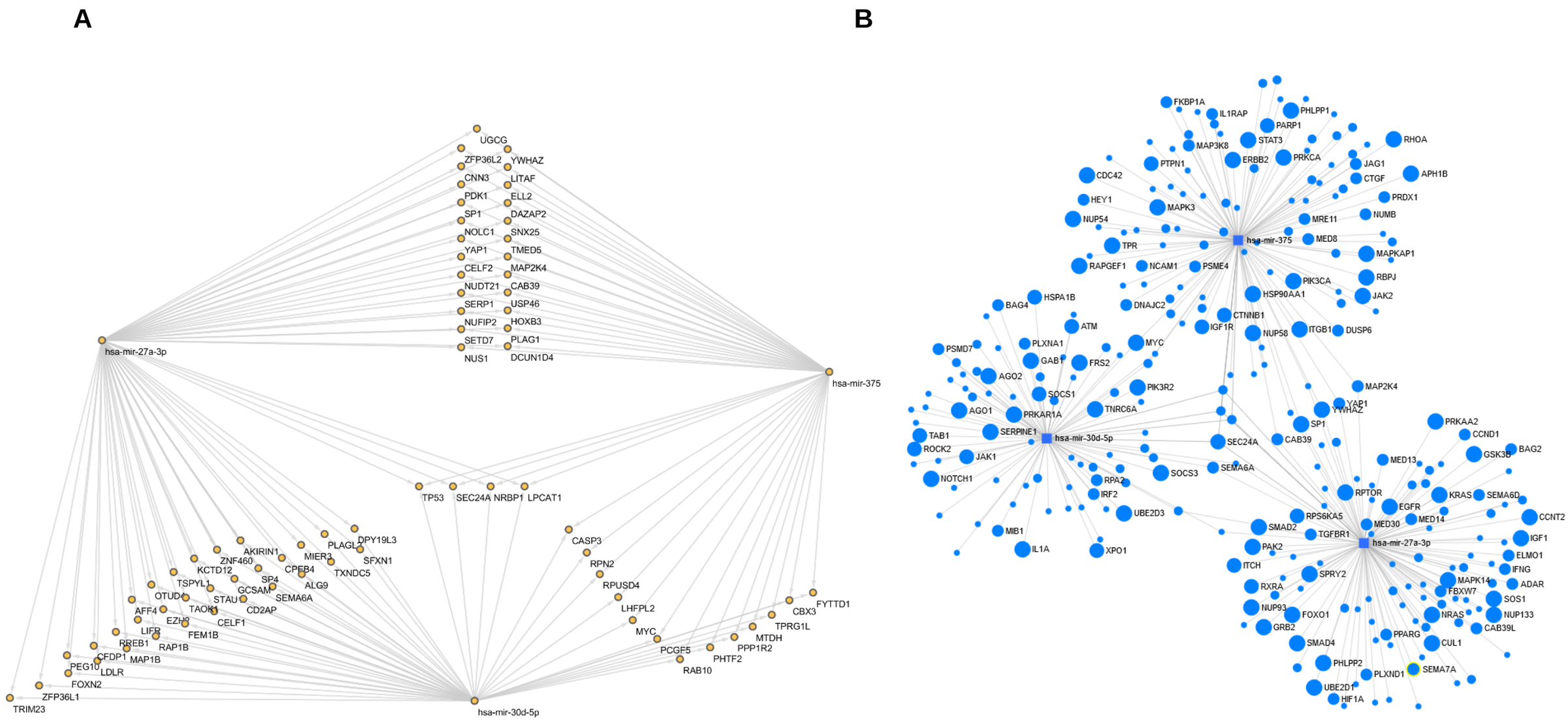

Supplemental Figure 5. miRNAseq analysis reveals intricate endometriosis specific miR375, 30d-5p, 27a-3p axis network. Bioinformatics tool miRNet and Cytoscape was used to develop functional interpretations from small RNAseq data. A node of annotated common genes that have binding sites shared among miR-30d-5p, 27a-3p, and 375 was developed and several key genes responsible for pro-inflammatory and pro-angiogenic signaling such as ZFP36L2 (anti-inflammatory), HOXB3 (pro-angiogenic) as well as TP53 (tumor suppressor) were identified (A). Reactome-computed interacting genes ($p<0.05$) of miR network reveal inflammation and angiogenesis genes shared among the miR network (B; larger circles, higher p value).

Biological Process Analysis

A

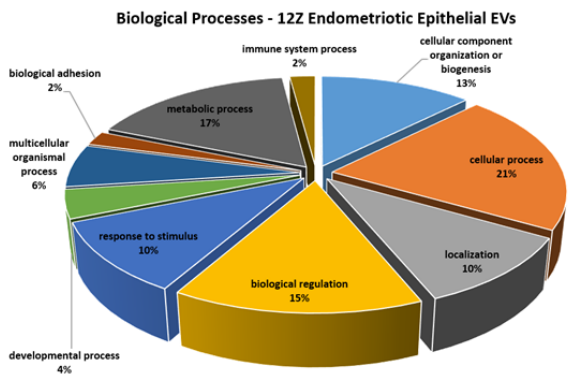

B

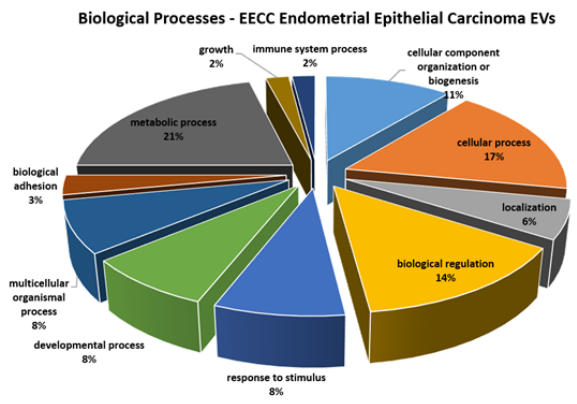

C

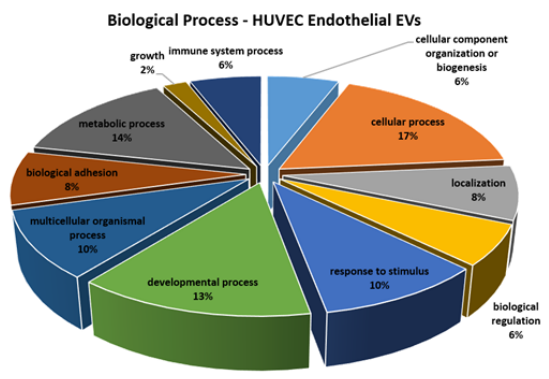

Molecular Function Analysis

D

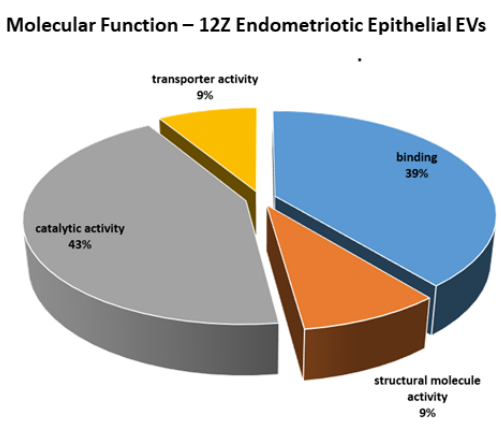

E

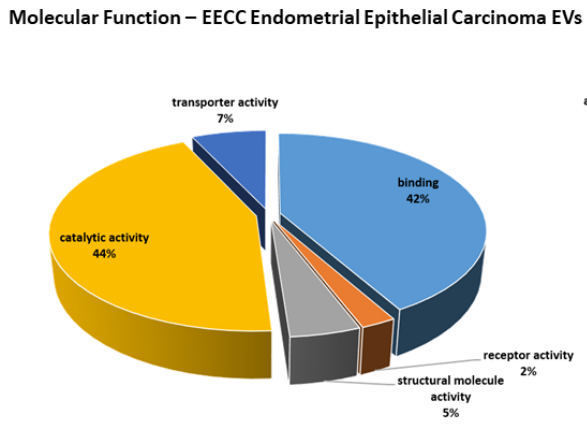

F

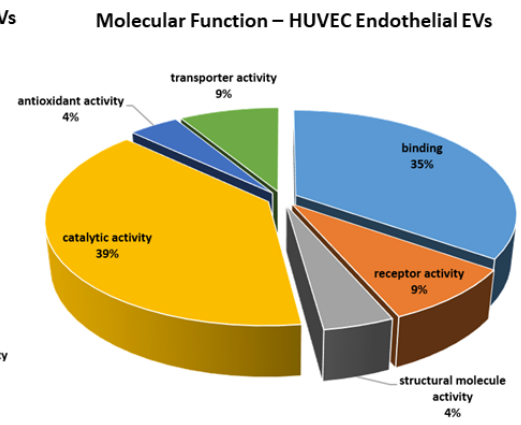

G

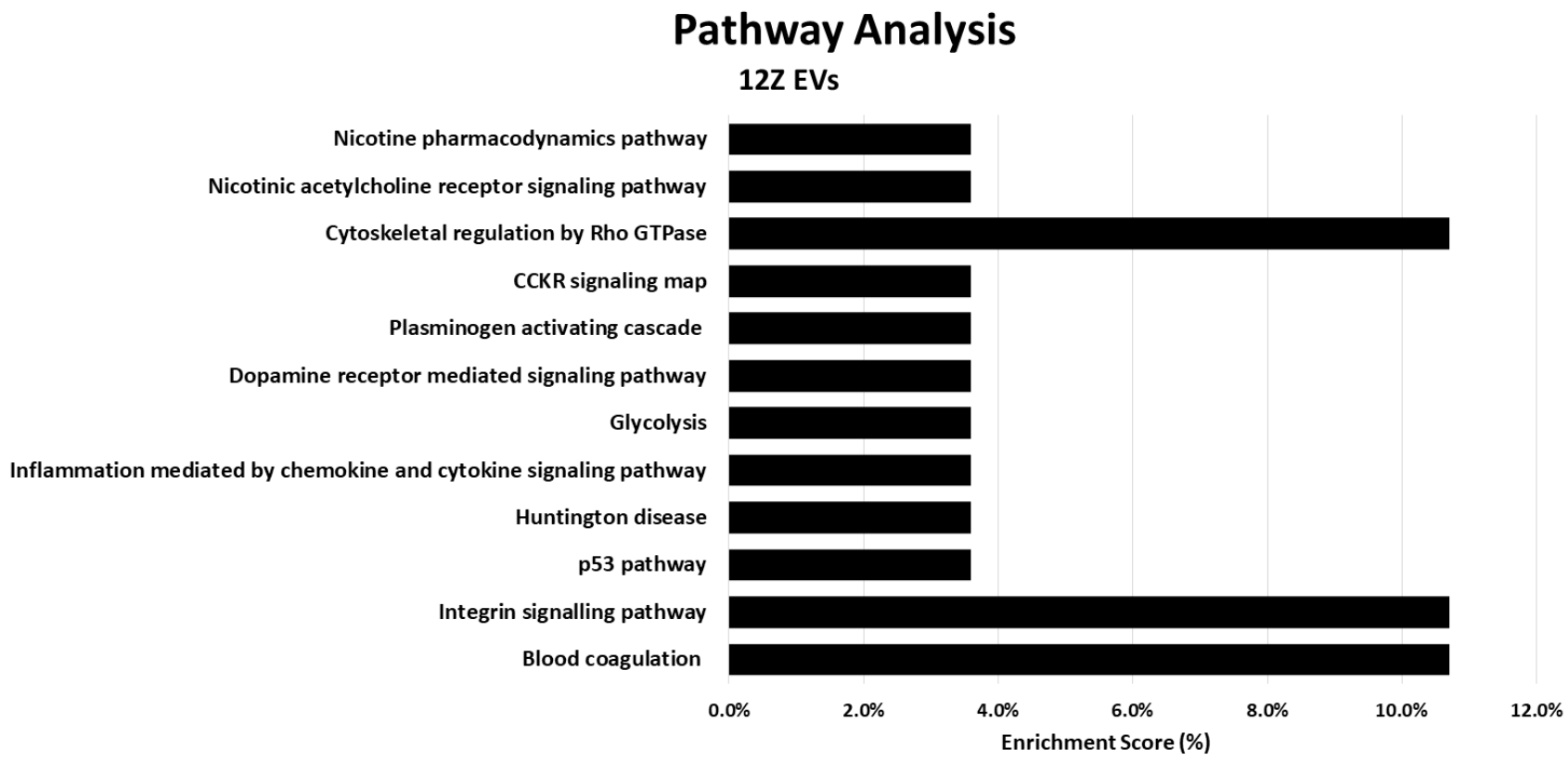

H

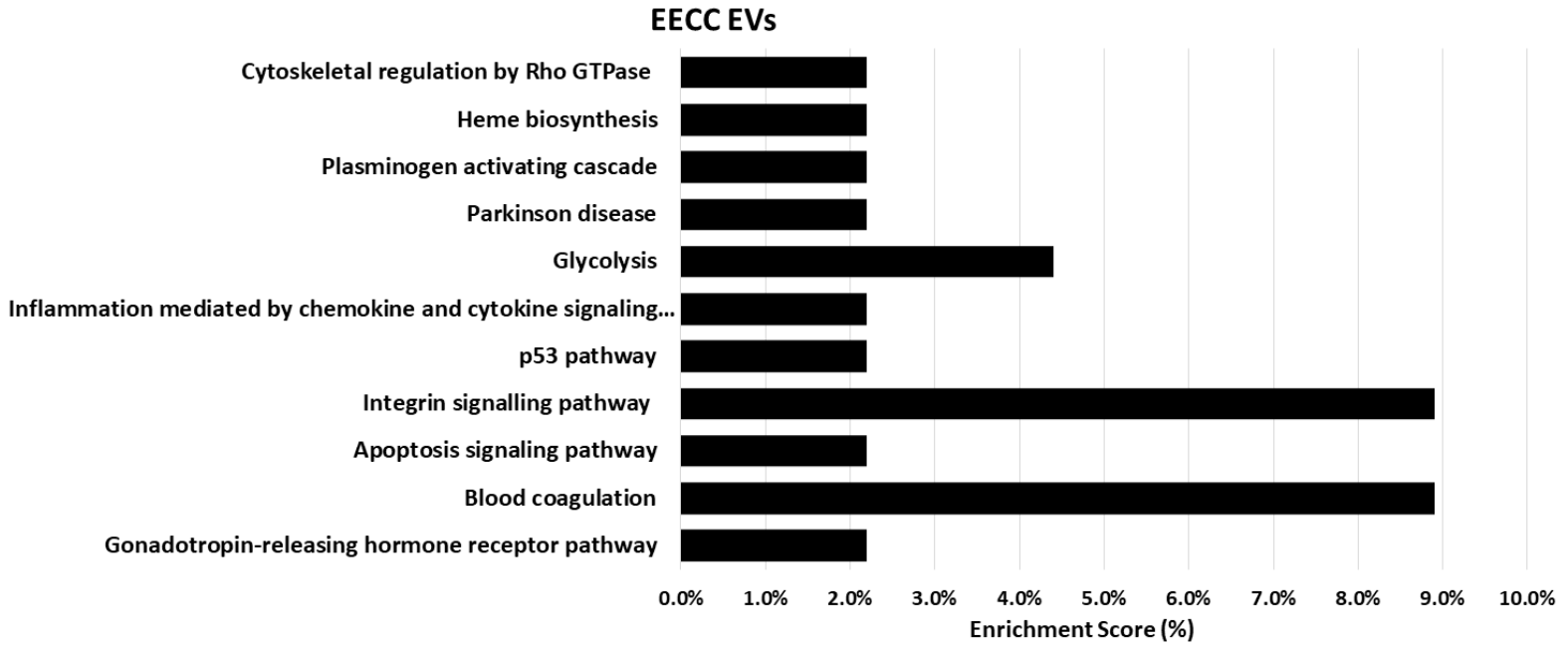

I

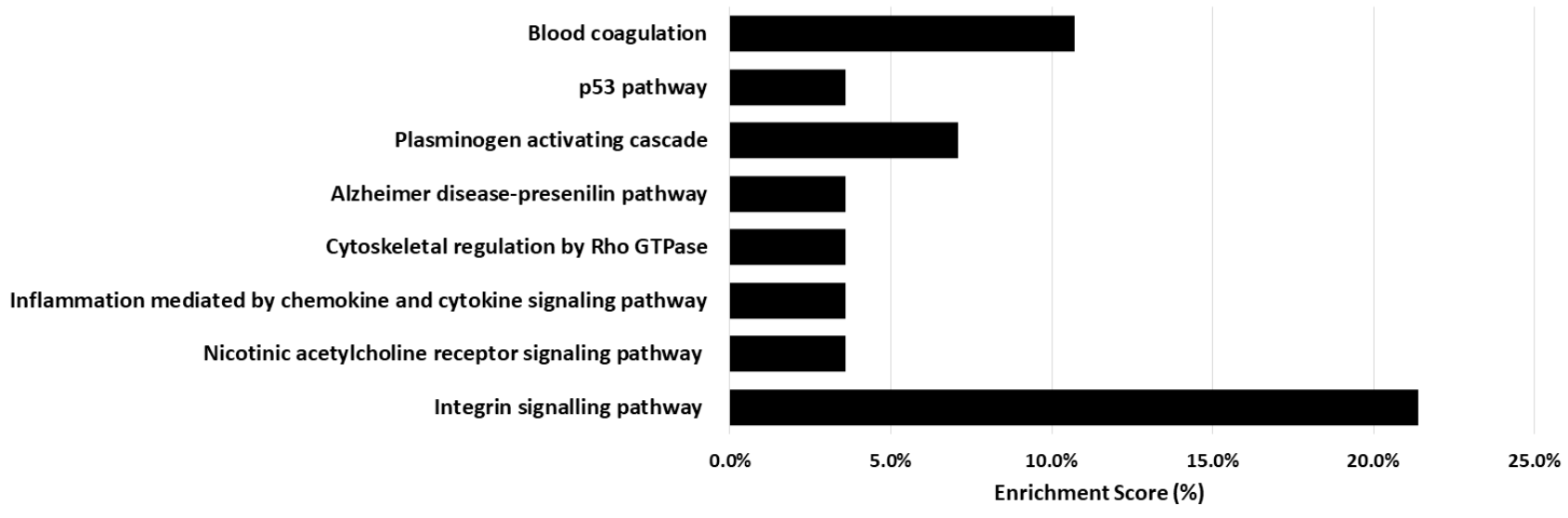

Supplemental Figure 6. 12Z Endometriotic and HUVEC EVs including exosomes using mass spectrometry. PantherDB gene ontology analysis was performed on EVs from cell lines and separated our findings based on biological process (A-C), molecular function (D-F) and pathways implicated (G-I). Biological process analysis in cell lines showed that HUVECs displaying higher developmental process, lower biological regulation, higher biological adhesion, and higher immune system process. 12Z display zero growth biological process (vs 2% in EECC and HUVECs; A-C). EECCs display higher metabolic process compared to both HUVECs and EECCs (A-C). Molecular function analysis of cell lines demonstrate that EECCs and 12Z endometriotic epithelial cells have similar molecular function profiles, with lower or no receptor activity compared to HUVECs (D-F). HUVECs displayed presence of antioxidant activity compared to the absence of this function in both 12Z and EECCs (D-F). Pathway analysis reveals that HUVEC EVs displayed higher grade integrin signaling pathway compared to 12Z and EECC EVs; EECCs displayed medium and 12Zs displaying lowest (G-I). 12Z EVs also have more cytoskeletal regulation by Rho GTPase compared to HUVECs and EECCs, and the CCKR signaling map pathway is present only in 12Z EVs (G). HUVECs have higher plasminogen activating cascade pathway compared to EECC and 12Z EVs (G-I). n = 5 biological replicates/group.

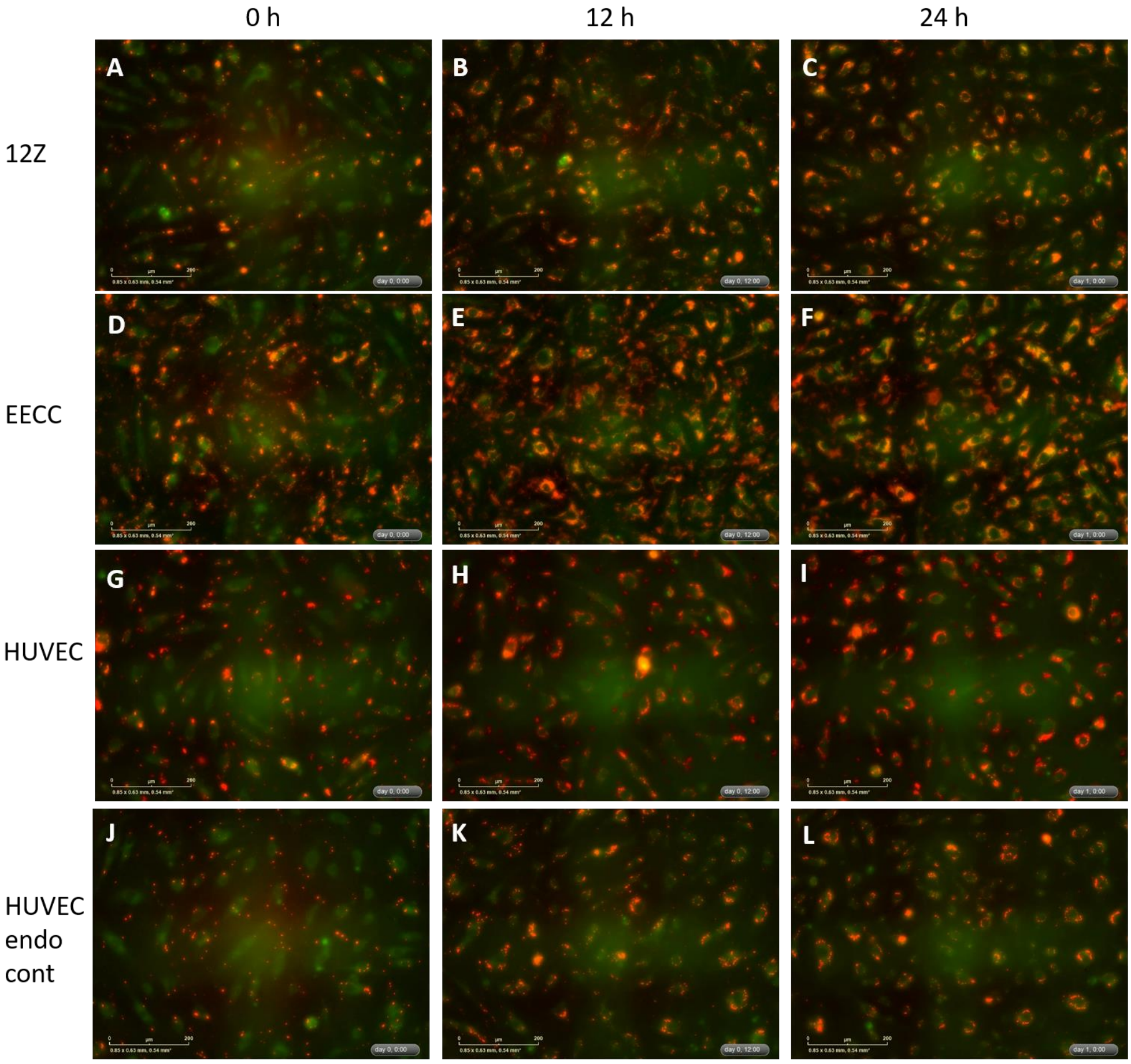

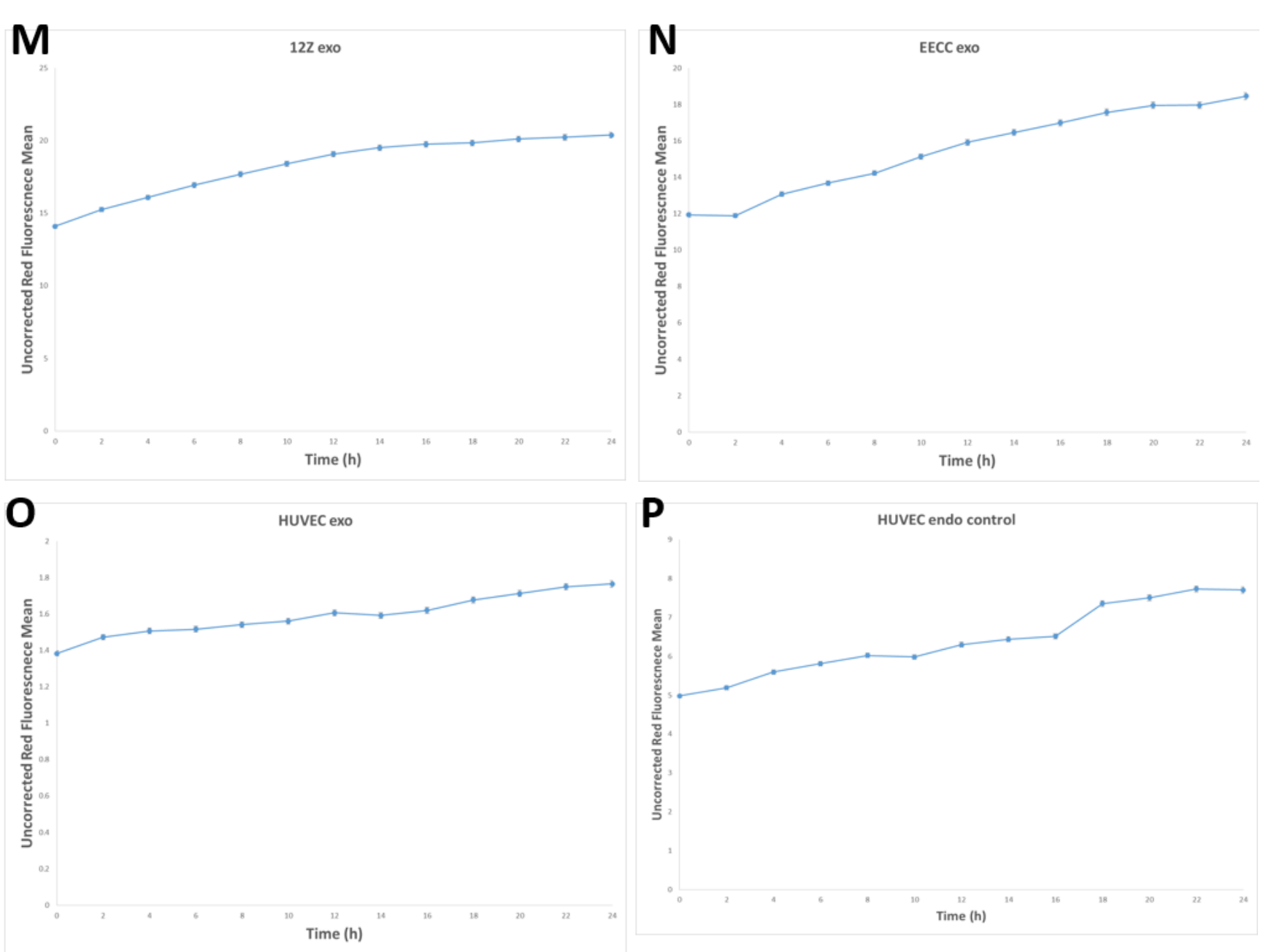

Supplemental Figure 7: Live cell imaging of endometriotic and endometrial epithelial-derived EV uptake demonstrate marked uptake in cytoplasm and nuclei in human endothelial cells. Live cell images using Incucyte of labelled EVs taken up in HUVEC recipient cells from 12Z (A-C), EECC (D-F), HUVEC (G-I) and negative (raw HUVEC supernatant labelled; no EV purification; J-L) at 0 h (A,D,G,J), 12h (B,E,H,K), and 24h (C,F,I,L). 12Z labelled EVs were found in moderate to high quantities in the cytoplasm of endothelial cells at 12 h (B), and high cytoplasmic levels were detected by 24 h (C). EECC labelled EVs were detected in high to very high levels in the cytoplasm and perinuclear space in endothelial cells at 12 and 24 h (E&F). HUVEC labelled EVs were detected in low to moderate quantities in the cytoplasm and nucleus of HUVECs, with gradual increasing by 24h (G-I). Negative endogenous control group had very minimal uptake compared to other groups from 0 – 24 h (J-L). 12Z (M), EECC (N), HUVEC (O) and negative endogenous control (P) fluorescence values from Incucyte were plotted from 0 – 24 h (M-P). n = 3 independent experiments.